Acta Crystallographica Section D
Biological Crystallography
ISSN 0907-4449

Structural basis of the histidine-mediated vitamin D receptor agonistic and antagonistic mechanisms of (23*S*)-25-dehydro-1α-hydroxyvitamin D_3-26,23-lactone

Shinji Kakuda,[a] Seiichi Ishizuka,[a,b] Hiroshi Eguchi,[a] Mathew T. Mizwicki,[c] Anthony W. Norman[c] and Midori Takimoto-Kamimura[a]*

[a]Teijin Institute for Bio-Medical Research, Japan, [b]Division of Hematology/Oncology, University of Pittsburgh School of Medicine, VA Pittsburgh Healthcare System (646), Research and Development (151-U), USA, and [c]Department of Biochemistry, University of California, USA

Correspondence e-mail: m.kamimura@teijin.co.jp

Received 26 March 2010
Accepted 1 June 2010

PDB References: vitamin D receptor–TEI-9647 complexes, 3a2h; 3a2i; 3a2j.

TEI-9647 antagonizes vitamin D receptor (VDR) mediated genomic actions of 1α,25$(OH)_2D_3$ in human cells but is agonistic in rodent cells. The presence of Cys403, Cys410 or of both residues in the C-terminal region of human VDR (hVDR) results in antagonistic action of this compound. In the complexes of TEI-9647 with wild-type hVDR (hVDRwt) and H397F hVDR, TEI-9647 functions as an antagonist and forms a covalent adduct with hVDR according to MALDI–TOF MS. The crystal structures of complexes of TEI-9647 with rat VDR (rVDR), H305F hVDR and H305F/H397F hVDR showed that the agonistic activity of TEI-9647 is caused by a hydrogen-bond interaction with His397 or Phe397 located in helix 11. Both biological activity assays and the crystal structure of H305F hVDR complexed with TEI-9647 showed that the interaction between His305 and TEI-9647 is crucial for antagonist activity. This study indicates the following stepwise mechanism for TEI-9647 antagonism. Firstly, TEI-9647 forms hydrogen bonds to His305, which promote conformational changes in hVDR and draw Cys403 or Cys410 towards the ligand. This is followed by the formation of a 1,4-Michael addition adduct between the thiol (–SH) group of Cys403 or Cys410 and the *exo*-methylene group of TEI-9647.

1. Introduction

Together with the nuclear vitamin D receptor (VDR), the steroid hormone 1α,25-dihydroxyvitamin D_3 [1α,25$(OH)_2D_3$; Fig. 1*a*] stimulates intestinal calcium absorption and increases bone calcium mobilization (Bouillon *et al.*, 1995; Carmeliet *et al.*, 2003; Hendy *et al.*, 2006; Lieberherr, 1987). They contribute to genomic and rapid responses, including the opening of

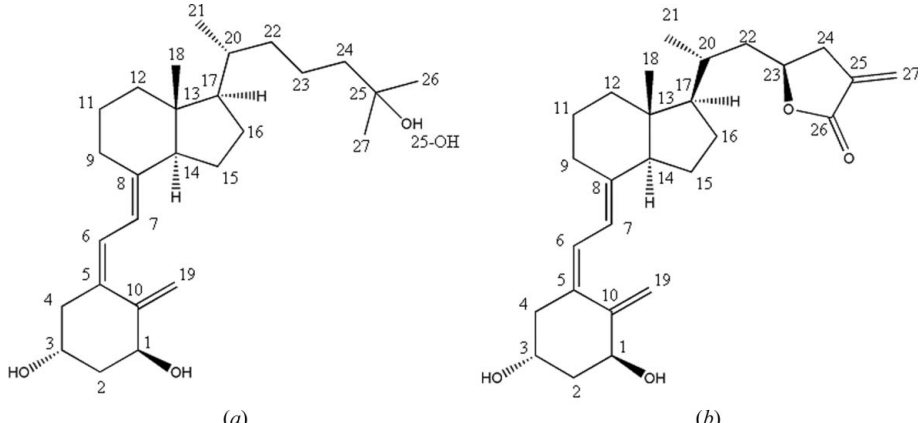

Figure 1
Structures of the vitamin D analogues discussed in this article. The chemical names of the analogues are as follows: (*a*) 1α,25$(OH)_2D_3$, 1α,25-dihydroxyvitamin D_3; (*b*) TEI-9647, (23*S*)-25-dehydro-1α-hydroxy-vitamin D_3-26,23-lactone.

voltage-gated calcium and chloride channels and MAPK activity (Norman, 1998; Song *et al.*, 1998; Zanello & Norman, 1997). The VDR is a ligand-dependent transcriptional regulator that like other nuclear receptors can activate genes by recruiting coactivators and the basal transcription machinery (Aranda & Pascual, 2001; O'Malley, 1990; Mangelsdorf *et al.*, 1995). Vitamin D_3 analogues can be classified as genomic agonists and antagonists based on their abilities to regulate reporter and endogenous genes that contain a vitamin D response element. Agonist compounds for the VDR provide therapeutic potential in the treatment of osteoporosis, psoriasis and secondary hyperparathyroidism (McKenna & O'Malley, 2002; Sutton & MacDonald, 2003). Antagonist compounds are being investigated as possible drugs for the treatment of Paget's disease (Ishizuka *et al.*, 2005).

The VDR contains three principal domains, a variable N-terminal domain that contains a ligand-independent activation function, a central highly conserved DNA-binding domain and a large C-terminal ligand-binding domain (LBD), with a short linker between the DNA-binding domain and the LBD. X-ray crystallograpic studies of the VDR LBD showed that it consists of 12 α-helices and three β-sheets. Helices 1–11 construct the ligand-binding pocket, whereas helices 3, 4 and 12 form the cofactor-binding pocket (Rochel *et al.*, 2000; Tocchini-Valentini *et al.*, 2001; Zanello & Norman, 2004). The DNA-bound closed helix 12 (H12) VDR conformer serves as a high-affinity scaffold for the recruitment of nuclear coactivators (Kalkhoven *et al.*, 1998; Rachez *et al.*, 1999). The current induced-fit model describing nuclear receptor activation is based on a comparison of apo and holo retinoid X receptor X-ray crystal structures. This nuclear receptor (NR) activation model posits that the closed transcriptionally active H12 conformation is induced by binding of the ligand to an open-like H12 apo NR conformer (Egea, Klaholz *et al.*, 2000; Egea, Mitschler *et al.*, 2000; Moras & Gronemeyer, 1998; Renaud & Moras, 2000).

A multitude of $1\alpha,25(OH)_2D_3$ analogues have been synthesized in recent years in an attempt to provide beneficial therapeutic agents. Chemical modifications of every portion of $1\alpha,25(OH)_2D_3$ have been reported (Stein & Wark, 2003). We have found that (23*S*)-25-dehydro-1α-hydroxyvitamin D_3-26,23-lactone (TEI-9647; Fig. 1*b*) functions to block VDR-mediated genomic actions of $1\alpha,25(OH)_2D_3$ (Ishizuka, Bannai *et al.*, 1981; Ishizuke, Yamaguchi *et al.*, 1981; Ishizuki *et al.*, 1984*a*,*b*; Ishizuka & Norman, 1987). One currently proposed mechanism suggests that the bulky side chain of TEI-9647 competitively inhibits VDR–$1\alpha,25(OH)_2D_3$ transactivation by strict hindrance of the closure of H12 of the VDR (Carlberg & Molnár, 2006; Perakyla *et al.*, 2004). The second currently proposed mechanism hinges on recent evidence indicating that TEI-9647 antagonism is species-specific and that the *exo*-methylene carbonyl structure of TEI-9647 is a very good Michael addition acceptor (Ochiai *et al.*, 2005). This has led to the proposal that the 25-methylene group of TEI-9647 can undergo a 1,4-Michael addition with Cys403 or Cys410 of the human VDR (hVDR). TEI-9647 antagonism disappears in rat VDR (rVDR) because Cys403 and Cys410 are replaced by Ser and Asn residues, respectively. Recently, molecular-modelling and structure–function studies have led to the proposal that TEI-9647 antagonism is rooted in the fact that the side chain has a reduced molecular volume compared with that of $1\alpha,25(OH)_2D_3$. This increases TEI-9647 side-chain mobility in the hVDR ligand-binding pocket, disrupting hydrophobic contacts with H12 and allowing the exocyclic methylene to form a covalent adduct with His305 (Mizwicki *et al.*, 2009). The detailed allostery underlying TEI-9647 antagonism of VDR–$1\alpha,25(OH)_2D_3$-mediated transactivation remains an important unresolved question in the light of the proposed use of TEI-9647 or analogues for the treatment of Paget's disease (Kurihara *et al.*, 2004). Mutation studies (H305F, H305F/H397F) in hVDR converted TEI-9647 from antagonist to agonist activity (Mizwicki *et al.*, 2007). Therefore, subtle structural changes both in the ligand and the receptor (*i.e.* mutations) result in drastic changes in activity.

In this study, we analyzed wild-type rVDR (rVDRwt), H305F and H305F/H397F hVDR complexed with TEI-9647 by X-ray crystallography. In addition, the complexes of TEI-9647 with wild-type hVDR (hVDRwt) and H397F hVDR in which TEI-9647 plays the role of an antagonist were analyzed by MALDI–TOF MS. Based on the results obtained, we provide a structural basis for the mechanisms of the vitamin D antagonistic and agonistic actions of TEI-9647.

2. Materials and methods

2.1. Cloning, expression and purification

The hVDRwt ligand-binding domain (LBD) (hVDRwt LBD; residues 118–427 Δ165–215) and the rVDRwt LBD (residues 116–423 Δ165–211) were amplified by PCR amplification from a full-length VDR expression construct with primers containing flanking restriction sites and inserted into pET28a (Novagen). The mutations (H305F, H397F, H305F/H397F) were created in pET28a-hVDRwt. The expression and purification of VDR LBD were performed essentially as described previously (Rochel *et al.*, 2000; Zanello & Norman, 2004; Vanhooke *et al.*, 2004). The VDR LBD was expressed as a His_6-fusion protein in *Escherichia coli* BL21 (DE3) by induction with 500 μM isopropyl β-D-1-thiogalactopyranoside (IPTG) at 293 K for 16 h. Cells were lysed in buffer containing 20 m*M* Tris–HCl pH 8.0, 100 m*M* NaCl, 10% glycerol, 5 m*M* β-mercaptoethanol and 20 mg ml^{-1} lysozyme by three freeze–thaw cycles. The supernatant from ultracentrifugation was purified by affinity chromatography using an Ni-Sepharose column (GE Biosciences). The resin was washed to remove unbound material according to the manufacturer's guidelines. The VDR LBD was eluted using buffer consisting of 20 m*M* Tris–HCl pH 8.0, 10% glycerol, 100 m*M* NaCl, 5 m*M* β-mercaptoethanol, 400 m*M* imidazole. The His_6 tag was removed from N-terminal constructs by thrombin cleavage (50 U thrombin per millilitre) overnight at 277 K. The cleaved protein was further purified using a gel-filtration column (GE Biosciences) equilibrated with 10 m*M* Tris–HCl pH 7.0,

Table 1
Data-collection and refinement statistics.

Values in parentheses are for the highest resolution shell.

Crystal	rVDRwt LBD–TEI-9647	H305F hVDR LBD–TEI-9647	H305F/H397F hVDR LBD–TEI-9647
Space group	*C*2	$P2_12_12_1$	$P2_12_12_1$
Unit-cell parameters (Å)			
a	124.81	44.80	44.69
b	45.35	51.37	51.39
c	46.66	131.77	131.85
Data collection			
Beamline	SLS X06SA	PF NW12	PF NW12
Wavelength (Å)	1.000	1.000	1.000
Resolution (Å)	50.00–2.50 (2.59–2.50)	50.00–3.25 (3.34–3.25)	50.00–2.70 (2.80–2.70)
Total No. of reflections	28263	34616	59192
Unique reflections	9008	5094	8852
$R_{\rm merge}$†	0.095 (0.252)	0.162 (0.349)	0.099 (0.324)
Completeness (%)	99.3 (96.4)	99.9 (100.0)	99.6 (99.2)
Multiplicity	3.1 (3.2)	3.8 (3.7)	3.7 (3.5)
Average $I/\sigma(I)$	8.2 (3.3)	14.0 (5.06)	20.6 (5.62)
Refined statistics			
R factor‡ (%)	22.9	21.8	22.5
$R_{\rm free}$‡ (%)	30.9	27.6	26.7
R.m.s. deviation from ideal values			
Bond lengths (Å)	0.010	0.006	0.006
Bond angles (°)	1.33	1.10	1.01
Ramachandran statistics			
Most favoured regions (%)	93.2	93.0	92.6
Additional allowed regions (%)	6.4	7.0	7.0
Generously allowed regions (%)	0.4	0.0	0.4
Disallowed regions (%)	0.0	0.0	0.0

† $R_{\rm merge} = \sum_{hkl}\sum_i |I_i(hkl) - \langle I(hkl)\rangle| / \sum_{hkl}\sum_i I_i(hkl)$, where $\langle I(hkl)\rangle$ is the mean intensity of *i* reflections with intensities $I_i(hkl)$ and common indices *hkl*. ‡ *R* factor = $\sum_{hkl} ||F_{\rm obs}| - |F_{\rm calc}|| / \sum_{hkl} |F_{\rm obs}|$, where $F_{\rm obs}$ and $F_{\rm calc}$ are the observed and calculated structure factors; $R_{\rm free}$ is calculated for a randomly chosen 5% of reflections and the *R* factor is calculated for the remaining 95% of reflections.

100 m*M* NaCl and 10 m*M* DTT (buffer I) and the protein was concentrated to above 10 mg ml^{-1}.

2.2. Crystallization, data collection and structure determination

Crystals of the H305F hVDR LBD–TEI-9647 and H305F/H397F hVDR LBD–TEI-9647 complexes formed in 1–2 d using the hanging-drop vapour-diffusion method with 0.1 *M* MES pH 6.5 and 1.2–1.6 *M* ammonium sulfate. We cocrystallized the rVDRwt LBD–TEI-9647 complex and a synthetic peptide containing the L*XX*LL sequence of the coactivator DRIP 205. The synthetic peptide (amino-acid sequence KNHPMLMNLLKDN-NH_2) was added to the rVDRwt LBD–TEI-9647 complex in a fivefold molar excess over the protein. rVDRwt LBD–TEI-9647 crystals were obtained using 1.2 *M* malonic acid pH 7.0 after two weeks. Crystals formed in 1–2 d using this technique, allowing optimization. These crystals were obtained by using a cat whisker to transfer microseeds of crystals of hVDRwt LBD–1α,25$(OH)_2D_3$ and rVDRwt LBD–1α,25$(OH)_2D_3$ in 1.4 *M* ammonium sulfate with 0.1 *M* MES pH 6.5. Prior to flash-freezing in liquid nitrogen, the hVDR crystals were transferred to a solution consisting of 0.1 *M* MES pH 6.5, 1.4 *M* ammonium sulfate and 30% glycerol. The rVDR crystals were transferred to a solution consisting of 1.2 *M* malonic acid pH 7.0 and 30% glycerol. Diffraction data were collected on beamline X06SA at the Swiss Light Source (SLS) and beamline NW12 at the Photon Factory (PF) and were processed with the *CrystalClear* software (Rigaku) and *HKL*-2000 (Otwinowski & Minor, 1997). The hVDRwt LBD–1α,25$(OH)_2D_3$ structure (PDB code 1db1; Rochel *et al.*, 2000) and the rVDRwt LBD–1α,25$(OH)_2D_3$ structure (PDB code 1rk3; Vanhooke *et al.*, 2004) were used as starting structures for molecular replacement using *MOLREP* (Vagin & Teplyakov, 1997) from the *CCP*4 suite (Collaborative Computational Project, Number 4, 1994). Refinement was carried out using the program *REFMAC* (Murshudov *et al.*, 1997). A sample containing a random 5% of the total reflections in the data set was excluded for $R_{\rm free}$ calculations. After rigid-body refinement, electron density for TEI-9647 was clearly constructed using *Coot* (Emsley & Cowtan, 2004). Figures were prepared with *DS Visualizer* (Accelrys; http://accelrys.co.jp/).

2.3. MALDI–TOF MS analysis

TEI-9647 was dissolved in absolute ethanol (EtOH) and incubated with 1 m*M* (final concentration) recombinant VDRs at a 10:1 compound:protein molar ratio for 1 h at room temperature. An equal volume of EtOH without TEI-9647 was used as a vehicle control. The reaction mixtures were desalted with C18 ZipTips (Millipore, Bedford, Massachusetts, USA), which also removed noncovalently bound TEI-9647. The reaction products were eluted with 5 µl acetic acid:acetonitrile:H_2O [0.1:49.95:49.95(*v*:*v*:*v*)] from the ZipTip. 1 µl purified reaction solution was mixed with 1 µl matrix solution (10 mg ml^{-1} sinnapinic acid) in acetic acid:acetonitrile:H_2O [0.1:49.95:49.95(*v*:*v*:*v*)] and loaded onto a 100-well matrix-assisted laser desorption ionization plate. A PerSeptive BioSystems Voyager STR MS with a high-mass detector and *Voyager NT* v.5.0 software (Framingham, Massachusetts, USA) was used for MALDI–TOF MS analysis. Calibration was performed with apomyoglobin using the $[M + H]^+$ = 16 952.6 Da and $[2M + H]^+$ = 33 904.0 Da ions. Data were collected in linear mode and 500 scans were averaged per spectrum.

2.4. Ligand-binding assays

The K_d of 1α,25$(OH)_2D_3$ for the hVDRwt LBD and the H305F, H397F and H305F/H397F hVDR LBDs was calculated as described previously (Ishizuka *et al.*, 1981). Briefly, the purified mutated hVDRs (each at 500 ng protein per millilitre of reaction buffer) were incubated with increasing amounts

of [26,27-methyl-^{3}H]-1α,25(OH)$_2$D$_3$ (specific activity of 5.846 TBq mmol^{-1}; 158 Ci mmol^{-1}; GE Biosciences) in the presence or absence of a 500-fold excess of nonlabelled 1α,25(OH)$_2$D$_3$ for 3 h at 277 K. The [^{3}H]-1α,25(OH)$_2$D$_3$ bound to the VDR was measured using the polyethylene glycol precipitation assay. The total binding represents bound [^{3}H]-1α,25(OH)$_2$D$_3$ in the absence of nonlabelled 1α,25(OH)$_2$D$_3$ and the nonspecific binding represents bound [^{3}H]-1α,25(OH)$_2$D$_3$ in the presence of a 500-fold excess of nonlabelled 1α,25(OH)$_2$D$_3$. Specific binding was calculated by subtracting the nonspecific binding from the total binding. The K_d of 1α,25(OH)$_2$D$_3$ for the mutated hVDR was calculated by Scatchard analysis of the specific binding of 1α,25(OH)$_2$D$_3$ as described previously (Ishizuka *et al.*, 1981).

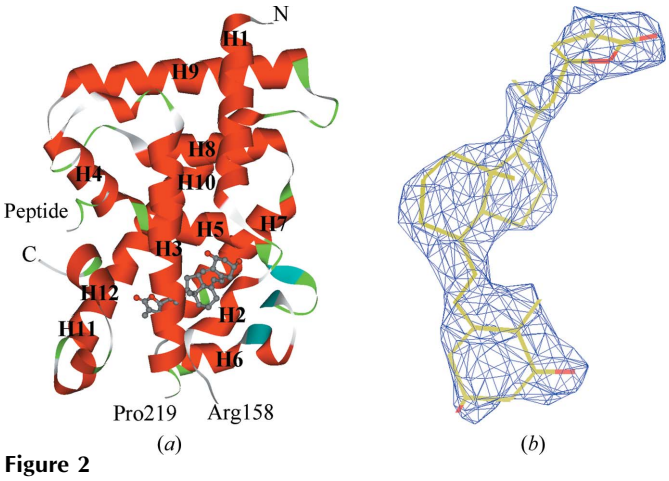

Figure 2
Structures and binding conformations of TEI-9647. The rVDRwt LBD–TEI-9647 complex demonstrates the same overall fold as the H305F and H305F/H397F hVDR LBD complexes. This finding is not surprising because this mutation imparts agonist activity to TEI-9647. The rVDRwt LBD complex superimposes on the H305F hVDR LBD complex with a root-mean-square deviation of 0.67 Å for all main-chain atoms. The rVDRwt LBD complex superimposes on the H305F/H397F hVDR LBD complex with a root-mean-square deviation of 0.64 Å for all main-chain atoms. (*a*) rVDRwt LBD–TEI-9647 complex. (*b*) TEI-9647 within the $F_o - F_c$ simulated-annealing OMIT map with TEI-9647 omitted.

3. Results and discussion

3.1. Overall protein structure

All the observed crystal forms were isomorphous, with no significant changes in the protein conformation. hVDRwt LBD complexed with TEI-9647 failed to crystallize under the conditions used to obtain the holo rVDRwt LBD, H305F hVDR and H305F/H397F hVDR crystals. Similar wild-type constructs have previously been used to solve the structures of rVDRwt LBD and hVDRwt LBD bound to 1α,25(OH)$_2$D$_3$ and to several synthetic ligands (Rochel *et al.*, 2000; Tocchini-Valentini *et al.*, 2001; Vanhooke *et al.*, 2004). The structures were solved by molecular replacement. The structures of the VDRs complexed with TEI-9647 were refined using usual methods and the experimental data and refinement statistics have been summarized in Table 1. After refinement of the protein alone, the map showed unambiguous electron density to which the ligand fitted. A ribbon representation of the

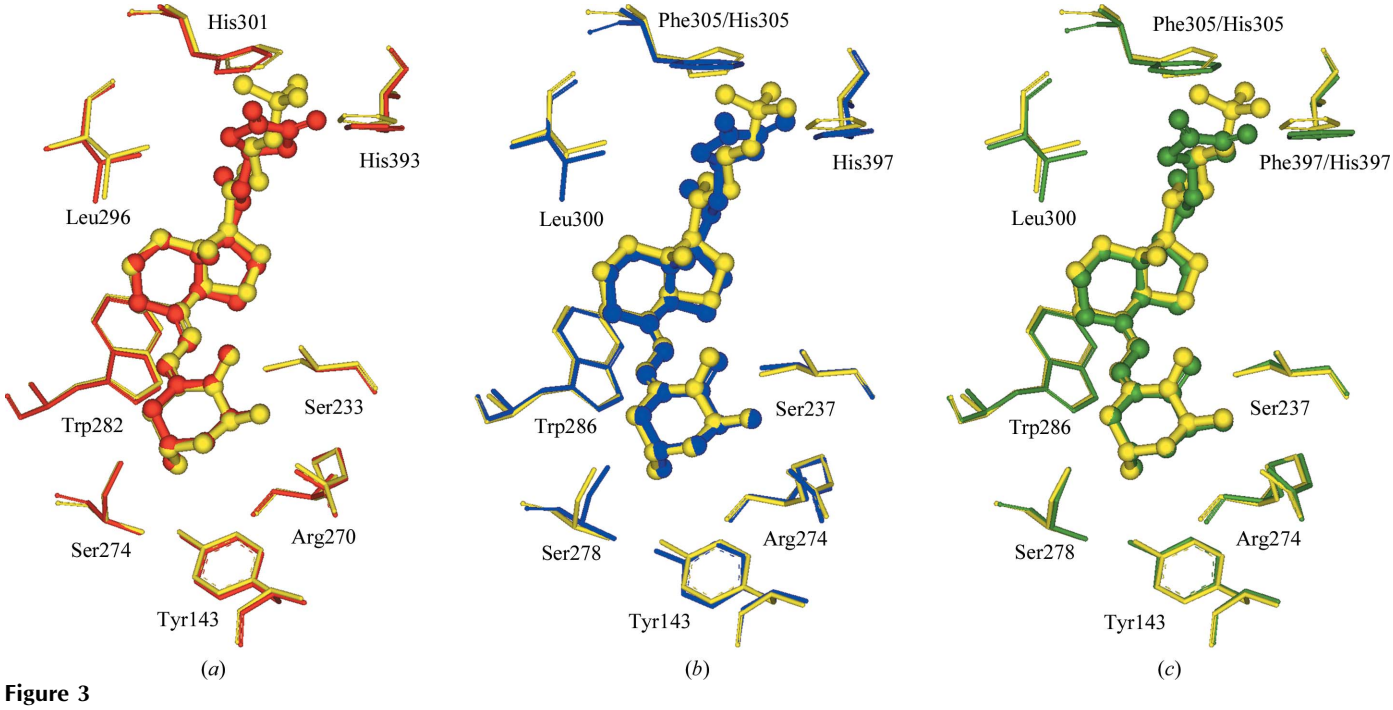

Figure 3
Ligand-binding pockets of superimposed structures of VDR LBD–TEI-9647 complexes and VDR LBD–1α,25(OH)$_2$D$_3$ complexes. The rVDRwt LBD–TEI-9647, H305F hVDR LBD–TEI-9647 and H305F/H397F hVDR LBD–TEI-9647 complexes are shown in red, blue and green and the VDR-1α,25(OH)$_2$D$_3$ complex is shown in yellow. In the A rings all the residues forming the binding pocket adopt the same conformation as in the rVDRwt LBD–1α,25(OH)$_2$D$_3$ structure. (*a*) The rVDRwt LBD–TEI-9647 complex superimposed onto rVDR–1α,25(OH)$_2$D$_3$ (PDB code 1rk3). (*b*) The H305F hVDR LBD–TEI-9647 complex superimposed onto hVDR–1α,25(OH)$_2$D$_3$ (PDB code 1bd1). (*c*) The H305F/H397F hVDR LBD–TEI-9647 complex superimposed onto hVDR–1α,25(OH)$_2$D$_3$ (PDB code 1bd1).

rVDRwt LBD–TEI-9647 complex is shown in Fig. 2(*a*). All previously reported nuclear receptor VDR LBD complexes adopt a canonical conformation with agonist bound, forming a three-layered sandwich containing 12–13 α-helices (Rochel *et al.*, 2000; Tocchini-Valentini *et al.*, 2001; Vanhooke *et al.*, 2004). Ligand OMIT maps calculated from the refined structure of

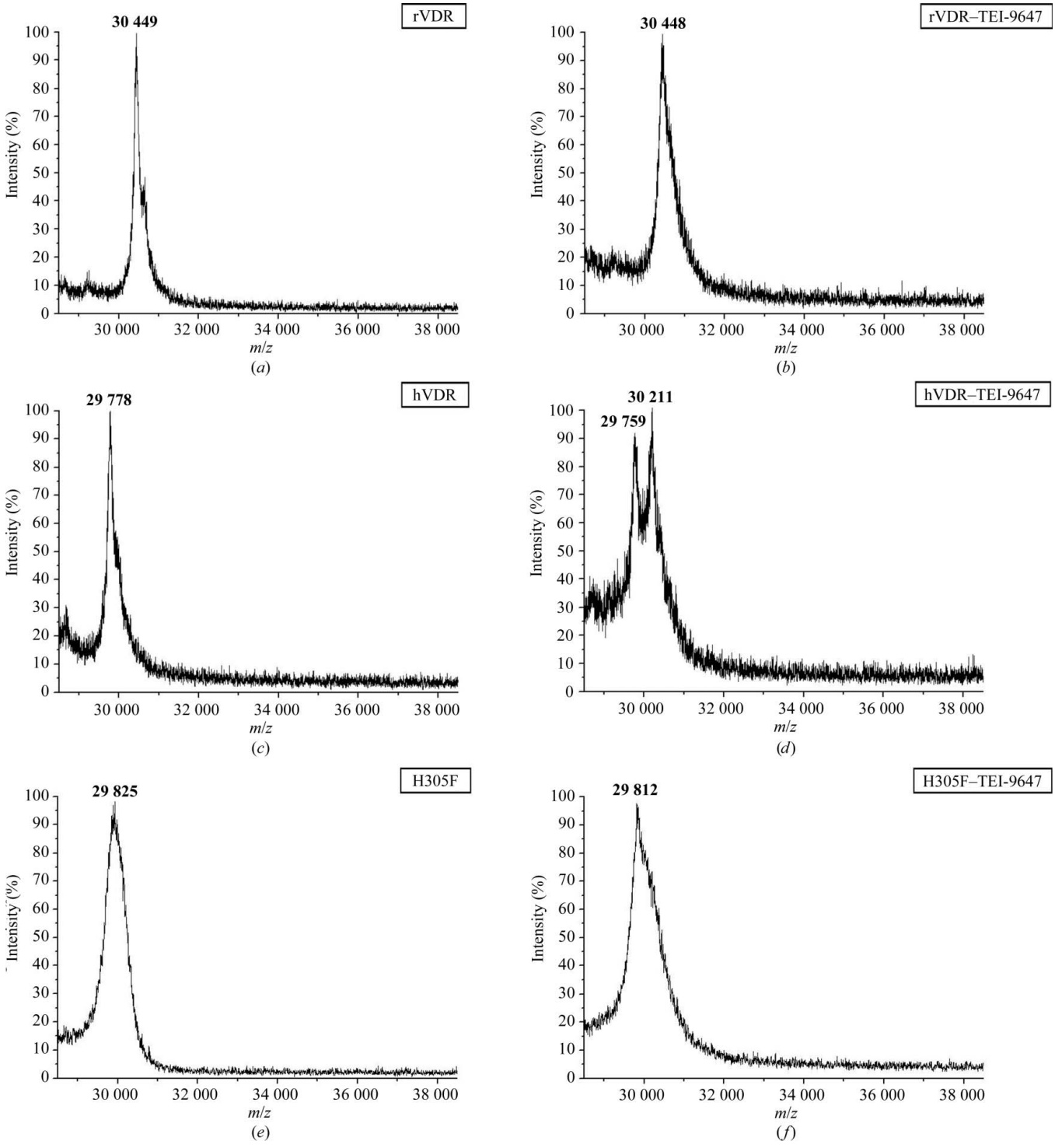

Figure 4
MALDI–TOF mass-spectrometric analysis of rVDRwt LBD, hVDRwt LBD and H305F, H397F and H305F/H397F hVDR LBDs bound by TEI-9647. (*a*) Mass spectrum of the reaction products from the rVDRwt LBD with EtOH vehicle. (*b*) Mass spectrum of the reaction products from the rVDRwt LBD with TEI-9647 at a 10:1 compound:protein molar ratio. (*c*) Mass spectrum of the reaction products from the hVDRwt LBD with EtOH vehicle. (*d*) Mass spectrum of the reaction products from the hVDRwt LBD with TEI-9647 at a 10:1 compound:protein molar ratio. (*e*) Mass spectrum of the reaction products from the H305F hVDR LBD with EtOH vehicle. (*f*) Mass spectrum of the reaction products from the H305F hVDR LBD with TEI-9647 at a 10:1 compound:protein molar ratio.

the rVDR LBD–TEI-9647 complex showed the ligand unequivocally (Fig. 2*b*). All the structures of rVDRwt and mutated hVDR showed the same structure as the usual VDR LBD structure bound by agonists. The classic conformation of the activated helix 12 was strictly conserved in all structures. The complexes of rVDRwt LBD, H305F and H305F/H397F hVDR LBD with TEI-9647 were aligned at C^{α} atoms with $1\alpha,25(OH)_2D_3$-bound complexes, with average root-mean-square (r.m.s.) deviations of 0.62, 0.30 and 0.36 Å, respectively. All of the ligands adopted the same orientation in the ligand-binding pocket.

3.2. Ligand-binding interactions

The interactions of rVDRwt LBD and H305F and H305F/H397F hVDR LBDs with TEI-9647 involve both hydrophobic contacts and electrostatic interactions. An adaptation of their conformation was observed in order to maintain the hydrogen bond forming the anchoring points. In the A ring of TEI-9647 hydrogen bonds are formed from 1-OH and 3-OH to Ser233/Arg270 (the corresponding residue numbers in human are Ser237/Arg274) and Tyr143/Ser274 (Tyr143/Ser278 in human), respectively. In rVDRwt LBD, 1-OH of TEI-9647 interacts with Ser233 and Arg270 (2.71 and 3.08 Å, respectively) and 3-OH interacts with Tyr143 and Ser274 (2.96 and 2.72 Å, respectively). In H305F hVDR LBD, 1-OH interacts with Ser237 and Arg274 (2.71 and 2.88 Å, respectively) and 3-OH interacts with Tyr143 weakly and with Ser278 (3.23 and 2.78 Å, respectively). In H305F/H397F hVDR LBD, 1-OH of TEI-9647 interacts with Ser237 and Arg274 (2.89 and 2.99 Å, respectively) and 3-OH interacts with Tyr143 and Ser278 (2.91 and 3.00 Å, respectively). These common interactions are shown in Fig. 3. When the rVDR LBD–TEI-9647 and rVDR LBD–$1\alpha,25(OH)_2D_3$ complexes were compared, the A, seco-B and C/D rings superimposed perfectly with only a 0.5 Å shift of the C/D rings (Fig. 3). The only major differences observed were the interactions formed with His301 and His393. His393 (2.89 and 2.81 Å, respectively) of rVDRwt LBD formed hydrogen bonds to two O atoms in the lactone ring of TEI-9647. In contrast, His301 (2.85 Å) and His393 (2.70 Å) in rVDRwt LBD interacted with 25-OH of $1\alpha,25(OH)_2D_3$. $1\alpha,25(OH)_2D_3$ showed a similar dissociation constant (K_d) in

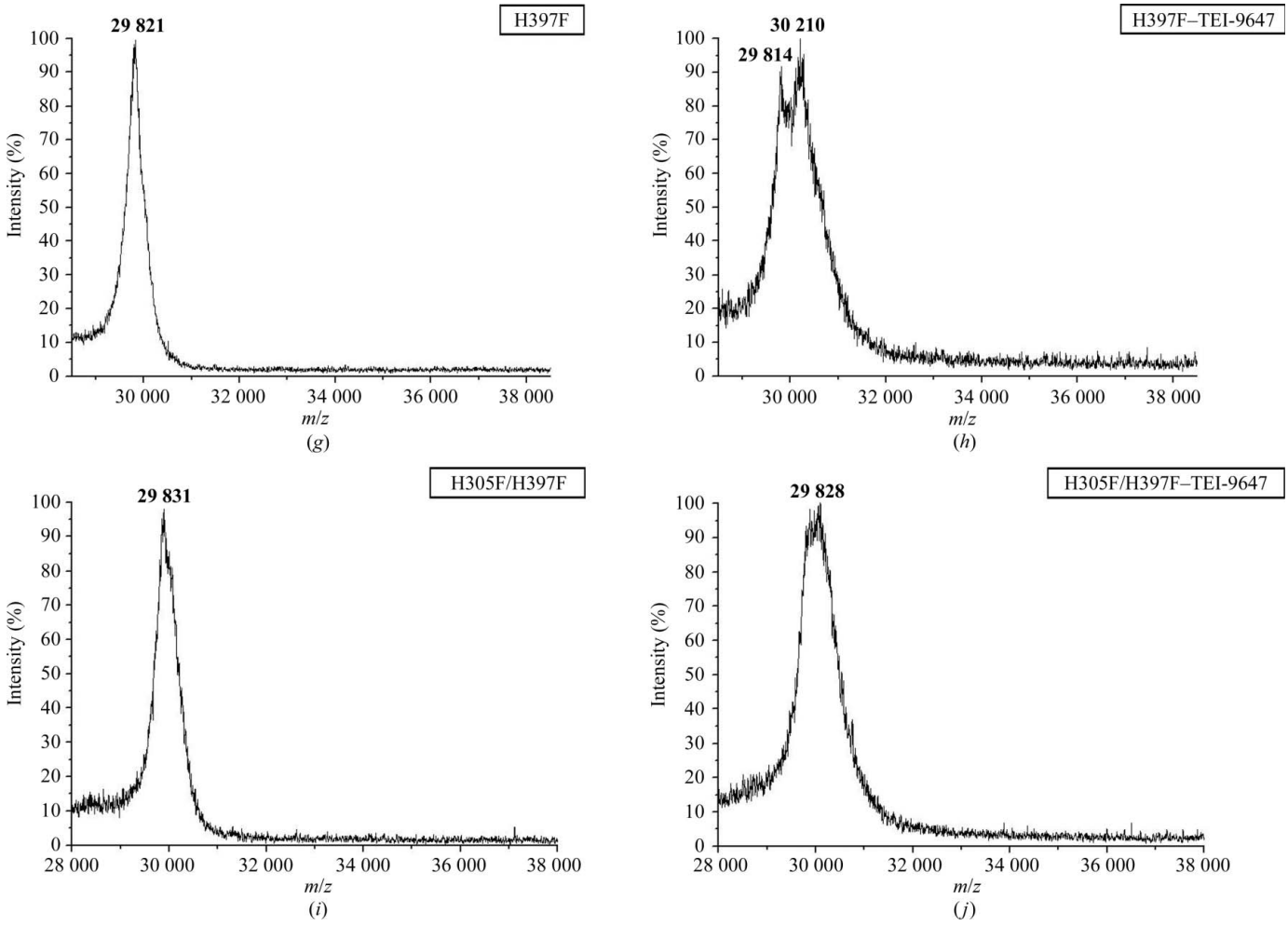

Figure 4 (continued)
(*g*) Mass spectrum of the reaction products from the H397F hVDR LBD with EtOH vehicle. (*h*) Mass spectrum of the reaction products from the H397F hVDR LBD with TEI-9647 at a 10:1 compound:protein molar ratio. (*i*) Mass spectrum of the reaction products from the H305F/H397F hVDR LBD with EtOH vehicle. (*j*) Mass spectrum of the reaction products from the H305F/H397F hVDR LBD with TEI-9647 at a 10:1 compound:protein molar ratio.

Table 2
Determination of K_d for binding of $1\alpha,25(OH)_2D_3$ to hVDRwt LBD and hVDR LBD mutants.

Binding-affinity values were determined as described in §2.

	K_d (M)
hVDRwt LBD	4.71×10^{-11}
H305F hVDR LBD	4.62×10^{-11}
H397F hVDR LBD	5.13×10^{-11}
H305F/H397F hVDR LBD	5.40×10^{-11}

the hVDR mutations, as shown in Table 2. In the H305F hVDR LBD–TEI-9647 complex, His397 (3.11 and 2.97 Å, respectively) formed hydrogen bonds to the two O atoms in the lactone ring of TEI-9647. In the H305F/H397F hVDR LBD–TEI-9647 complex, TEI-9647 formed π-interactions with the aromatic *R* groups of Phe305 and Phe397, consistent with modelling results (3.28 Å). In contrast, 25-OH of the natural ligand $1\alpha,25(OH)_2D_3$ interacted with His305 (2.81 Å) and His397 (2.82 Å) in the hVDRwt LBD. Thus, the two O atoms in the lactone ring of TEI-9647 clearly play different roles compared with the 25-OH of the natural ligand. They only formed hydrogen bonds to His397 (the corresponding residue in rat is His393), not to His305. These results suggest that the characteristic agonist and antagonist mechanisms of TEI-9647 are predicated on how TEI-9647 and $1\alpha,25(OH)_2D_3$ differentially interact with His301/His305 and His393/His397.

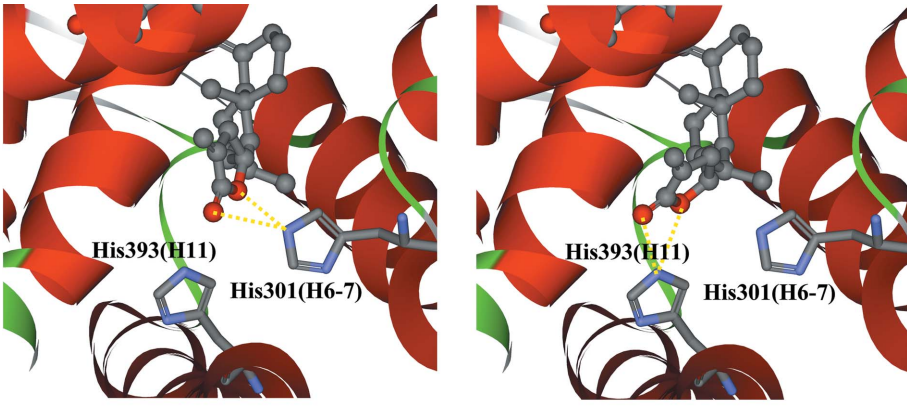

(*a*) (*b*)

Figure 5
Molecular modelling of TEI-9647, which interacts with His301 or His393 in rVDR. Molecular modelling was performed by least-squares fitting of the A, B and D rings of the TEI-9647 of the rVDRwt LBD–TEI-9647 complex structure. C atoms 2, 5, 8, 12, 14 and 17 were used in the fitting procedure. Because two O atoms of TEI-9647 are important for binding, they were placed at a position near to His301 of the receptor. Energy minimizations of the rVDRwt LBD–TEI-9647 complexes were performed using the TRIPOS force field and conjugate-gradient optimization methods with a convergence criterion requiring a minimum energy change of 0.004 kJ mol^{-1}. In the minimizations, the coordinates of the analogues, the protein and water molecules within 8.0 Å of the analogue atoms were allowed to move. The minimized complexes were visually checked. If there were bad contacts in the structures or several alternative ways to place the analogue side chain in the binding site, additional minimizations were carried out using different starting geometries. (*a*) TEI-9647 and the His301 (the corresponding residue number in human is His305) residue interact with the two O atoms in the lactone ring in the rVDRwt LBD–TEI-9647 docking model structure. (*b*) TEI-9647 and the His393 (the corresponding residue number in human is His397) residue interact with the two O atoms in the lactone ring in the rVDRwt LBD–TEI-9647 X-ray structure. TEI-9647 formed hydrogen bonds with His301 and His393 in the same relative steric space within the VDR ligand-binding pocket. The interaction with His393 plays an important role in stabilizing the H12 closed active conformation.

3.3. Ligand interactions with Cys403 or Cys410

We examined whether TEI-9647 (M_r = 427) could form a covalent VDR adduct with the rVDRwt LBD, hVDRwt LBD and H305F, H397F and H305F/H397F hVDR LBDs by mass-spectrometric techniques. We obtained MALDI–TOF signals of m/z = 30 449 ± 40 for rVDRwt LBD, m/z = 29 778 ± 40 for hVDRwt LBD, m/z = 29 825 ± 40 for H305F hVDR LBD, m/z = 29 821 ± 40 for H397F hVDR LBD and m/z = 29 831 ± 40 for H305F/H397F hVDR LBD after incubation with EtOH (Figs. 4*a*, 4*c*, 4*e*, 4*g* and 4*i*). When TEI-9647 was incubated with hVDRwt LBD and H397F hVDR LBD in a tenfold molar excess, the MALDI–TOF MS spectrum exhibited an increase in peak width and new base-peak mass assignments of 30 211 ± 50 and 30 210 ± 50 Da (Figs. 4*d* and 4*h*). The front shoulder of the main peak was assigned as free hVDRwt LBD (29 759 ± 50 Da) and the back shoulder of the main peak was assigned as hVDRwt LBD–TEI-9647 (30 211 ± 50 Da). The difference between the two peaks suggested that TEI-9647 binds to Cys403 or Cys410 of hVDR LBD at this compound:protein molar ratio (1:1). We tried to measure partial or complete proteolytic digestion of hVDRwt LBD–TEI-9647 using q-TOF mass spectrometry but were unsuccessful. The reason was considered to be that TEI-9647 was too large compared with the digested hVDRwt LBD fragment size to decide the matrix with q-TOF mass spectrometry. In contrast, we tried to measure C403S and C410N hVDR–TEI-9647 with MALDI–TOF MS and detected two peaks similar to those of hVDRwt LBD described above. These results support the hypothesis that the ability of TEI-9647 to antagonize genomic responses in the hVDR LBD results from TEI-9647 forming a covalent Michael adduct with either Cys403 or Cys410 of hVDR. These two residues are Ser and Asn in the rVDR molecule, respectively.

3.4. Agonistic and antagonistic mechanisms

All of the reported structures of VDR LBD with agonists are virtually identical. The molecular structures of VDR LBDs take the most stable conformation in the complex crystals. TEI-9647 interacted selectively with only His393 (His397 in human) in rVDRwt as an agonist even though rVDRwt also has two histidine residues (His301 and His393) that are proximal to the ligand side-chain atoms in the ligand-binding pocket. The His393 (His397 in human) residue is located in helix 11 (H11), which is under helix 12 (H12). Helices 3, 4 and 12 form the cofactor-binding pocket. We expected that interaction with His393 (His397 in human) plays

an important role in the agonistic mechanism of VDR LBD with TEI-9647 leading to a stable conformation and that the hydrogen bonds to His393 (His397 in human) are the key interaction that promotes the correct folding of helix 12. In contrast to the agonistic mode, we expect that TEI-9647 can bind to His301 (His305 in human) as an antagonist spatially, as shown by the molecular simulation results in Fig. 5(*a*). This has been previously demonstrated using modelling techniques that assess the dynamics of the interaction between TEI-9647 and the hVDR residues lining the ligand-binding pocket (Mizwicki *et al.*, 2009). In the H305F/H397F hVDR LBD, Phe397 replaced His397 to stabilize the conformation of H12, but no covalent adduct was observed. The lack of observation of any covalent adduct in the H305F constructs was consistent with the possibility that the residue functions as a molecular anchor for the formation of the adduct between TEI-9647 and Cys403 or Cys410 in the hVDR. In the other nuclear receptor example, oestrogen and glucocorticoid receptors, antagonists of these receptors sterically block H12 closure by interacting with H11 and H12. Cys403 of hVDR is located in H11 and Cys410 is located between H11 and H12. To evaluate whether the approach to the transition state of the TEI-9647 covalent adduct with Cys403 or Cys410 could be observed, we superimposed hVDR on the rVDR LBD–TEI-9647 complex. If hVDR adopts a similar structure with respect to rVDR the

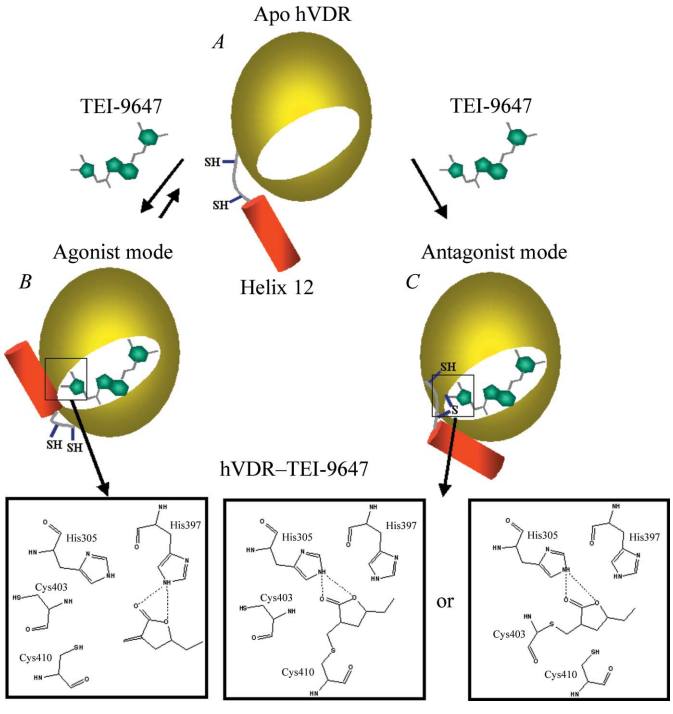

Figure 6
Agonist and antagonist switching mechanism of VDR with TEI-9647. The dynamic conformational heterogeneity of H12 of hVDR (modes A, B and C) is projected using nuclear receptor X-ray data. It is observed that in the hVDR apo structure H12 takes on an opened conformation. While it is proposed that in the hVDR mode B agonist structure H12 is bound to the coactivator surface, in hVDR mode C, the covalently bonded structure with TEI-9647, H12 is flexible. The difference in the population of the three H12 conformers causes the agonist and antagonist switching mechanism of the VDR with TEI-9647.

1α,25(OH)$_2$D$_3$ C27 atoms of the *exo*-methylene group of TEI-9647 will lie within 8.2 Å perpendicular to the Cys410 thiol S atom and within 13.4 Å perpendicular to the Cys403 thiol S atom. These distances are definitely too large for Michael addition between the thiol group of Cys403/Cys410 and the *exo*-methylene group of TEI-9647. The H305F and H305F/H397F hVDR LBD complexes did not make any interactions between the two O atoms of the lactone ring and Phe305. In the H305F hVDR LBD construct, the thiol S atom of Cys403 is 8.6 Å away and that of Cys410 is 13.7 Å away from the C27 atom of the *exo*-methylene group. In the H305F/H397F hVDR LBD, C27 of the *exo*-methylene group is at similar distances from the thiol S atoms of Cys403 and Cys410 (8.5 and 14.0 Å, respectively). We expect that the hydrogen-bonding interaction with His305 could be a trigger that causes the conformational change of hVDR and draws in the Cys403/Cys410, producing covalent bonding between TEI-9647 and Cys403/Cys410 by a 1,4-Michael addition.

4. Conclusions

The crystal structure with an antagonist-binding hVDR conformation should be different from those bound by the agonist because of the large conformational change of H12 that can be seen, for example, in the ERα structure with raloxifene and tamoxifen (Shiau *et al.*, 1998, 2002) and in the GR structure with RU-486 (Kauppi *et al.*, 2003). In this case, the binding of the antagonist to the hVDR LBD results in displacement of helix 12 so that it prohibits binding of the coactivator. From the present experimental results and the synthetic derivatization around TEI-9647, we propose a stepwise mechanism of TEI-9647 antagonism. In the first step, TEI-9647 forms hydrogen bonds to His305, which promote the change in the conformation of hVDR and draw in Cys403 or Cys410. As the final stage, a covalent bond should be created between the thiol group of Cys403/Cys410 and the *exo*-methylene group of TEI-9647 by a 1,4-Michael addition (Fig. 6).

In summary, given that TEI-9647 is a drug candidate for the treatment of Paget's disease and that it inhibits the calcium metabolism induced by 1α,25(OH)$_2$D$_3$, the finding that TEI-9647 can be turned into an agonist or a complete antagonist for which no 1α,25(OH)$_2$D$_3$ reporter activity is observed (Mizwicki *et al.*, 2009) could be of potential use therapeutically. In this study, we have shown that the antagonist mechanism of TEI-9647 is based upon its ability to induce a conformational change of hVDR by forming hydrogen bonds to His305, allowing the formation of a covalent bond to Cys403 or Cys410. These findings also provide new molecular tools for studying the structure–function relationship of hVDR and may lead to the design of a new type of agonist/antagonist and/or better analogues than TEI-9647.

References

Aranda, A. & Pascual, A. (2001). *Physiol. Rev.* **81**, 1269–1304.
Bouillon, R., Okamura, W. H. & Norman, A. W. (1995). *Endocr. Rev.* **16**, 200–257.

Carlberg, C. & Molnár, F. (2006). *Curr. Topics Med. Chem.* **6**, 1243–1253.
Carmeliet, G., Van Cromphaut, S., Daci, E., Maes, C. & Bouillon, R. (2003). *Best Pract. Res. Clin. Endocrinol. Metab.* **17**, 529–546.
Collaborative Computational Project, Number 4 (1994). *Acta Cryst.* D**50**, 760–763.
Egea, P. F., Klaholz, B. P. & Moras, D. (2000). *FEBS Lett.* **476**, 62–67.
Egea, P. F., Mitschler, A., Rochel, N., Ruff, M., Chambon, P. & Moras, D. (2000). *EMBO J.* **19**, 2592–2601.
Emsley, P. & Cowtan, K. (2004). *Acta Cryst.* D**60**, 2126–2132.
Hendy, G. N., Hruska, K. A., Mathew, S. & Goltzman, D. (2006). *Kidney Int.* **69**, 218–223.
Ishizuka, S., Bannai, K., Naruchi, T. & Hashimoto, Y. (1981). *Steroids*, **37**, 33–43.
Ishizuka, S., Ishimoto, S. & Norman, A. W. (1984*a*). *J. Steroid Biochem.* **20**, 611–615.
Ishizuka, S., Ishimoto, S. & Norman, A. W. (1984*b*). *Biochemistry*, **23**, 1473–1478.
Ishizuka, S., Kurihara, N., Reddy, S. V., Cornish, J., Cundy, T. & Roodman, G. D. (2005). *Endocrinology*, **146**, 2023–2030.
Ishizuka, S. & Norman, A. W. (1987). *J. Biol. Chem.* **262**, 7165–7170.
Ishizuka, S., Yamaguchi, H., Yamada, S., Nakayama, K. & Takayama, H. (1981). *FEBS Lett.* **134**, 207–211.
Kalkhoven, E., Valentine, J. E., Heery, D. M. & Parker, M. G. (1998). *EMBO J.* **17**, 232–243.
Kurihara, N., Ishizuka, S., Demulder, A., Menaa, C. & Roodman, G. D. (2004). *J. Steroid Biochem. Mol. Biol.* **89–90**, 321–325.
Kauppi, B. *et al.* (2003). *J. Biol. Chem.* **278**, 22748–22754.
Lieberherr, M. (1987). *Biol. Chem.* **262**, 13168–13173.
Mangelsdorf, D. J., Thummel, C., Beato, M., Herrlich, P., Schütz, G., Umesono, K., Blumberg, B., Kastner, P., Mark, M., Chambon, P. & Evans, R. M. (1995). *Cell*, **83**, 835–839.
McKenna, N. J. & O'Malley, B. W. (2002). *Cell*, **108**, 465–474.
Mizwicki, M. T., Bula, C. M., Bishop, J. E. & Norman, A. W. (2007). *J. Steroid Biochem. Mol. Biol.* **103**, 243–262.
Mizwicki, M. T., Bula, C. M., Mahinthichaichan, P., Henry, H. L., Ishizuka, S. & Norman, A. W. (2009). *J. Biol. Chem.* **284**, 36292–36301.
Moras, D. & Gronemeyer, H. (1998). *Curr. Opin. Cell Biol.* **10**, 384–391.
Murshudov, G. N., Vagin, A. A. & Dodson, E. J. (1997). *Acta Cryst.* D**53**, 240–255.
Norman, A. W. (1998). *J. Bone Miner. Res.* **13**, 1360–1369.
Ochiai, E., Miura, D., Eguchi, H., Ohara, S., Takenouchi, K., Azuma, Y., Kamimura, T., Norman, A. W. & Ishizuka, S. (2005). *Mol. Endocrinol.* **19**, 1147–1157.
O'Malley, B. W. (1990). *Mol. Endocrinol.* **4**, 363–369.
Otwinowski, Z. & Minor, W. (1997). *Methods Enzymol.* **276**, 307–326.
Perakyla, M., Molnar, F. & Carlberg, C. (2004). *Chem. Biol.* **11**, 1147–1156.
Rachez, C., Lemon, B. D., Suldan, Z., Bromleigh, V. & Gamble, M. (1999). *Nature (London)*, **398**, 824–828.
Renaud, J.-P. & Moras, D. (2000). *Cell. Mol. Life Sci.* **57**, 1748–1769.
Rochel, N., Wurtz, J. M., Mitschler, A., Klaholz, B. & Moras, D. (2000). *Mol. Cell*, **5**, 173–179.
Shiau, A. K., Barstad, D., Radek, J. T., Meyers, M. J., Nettles, K. W., Katzenellenbogen, B. S., Katzenellenbogen, J. A., Agard, D. A. & Greene, G. L. (2002). *Nature Struct. Biol.* **9**, 359–364.
Shiau, A. K., Barstad, D., Loria, P. M., Cheng, L., Kushner, P. J., Agard, D. A. & Greene, G. L. (1998). *Cell*, **95**, 927–937.
Song, X., Bishop, J. E., Okamura, W. H. & Norman, A. W. (1998). *Endocrinology*, **139**, 457–465.
Stein, M. S. & Wark, J. D. (2003). *Expert Opin. Invest. Drugs*, **12**, 825–840.
Sutton, A. L. & MacDonald, P. N. (2003). *Mol. Endocrinol.* **17**, 777–791.
Tocchini-Valentini, G., Rochel, N., Wurtz, J. M., Mitschler, A. & Moras, D. (2001). *Proc. Natl Acad. Sci. USA*, **98**, 5491–5496.
Vagin, A. & Teplyakov, A. (1997). *J. Appl. Cryst.* **30**, 1022–1025.
Vanhooke, J. L., Benning, M. M., Bauer, C. B., Pike, J. W. and DeLuca, H. F. (2004). *Biochemistry*, **43**, 4101–4110.
Zanello, L. P. & Norman, A. W. (1997). *J. Biol. Chem.* **272**, 22617–22622.
Zanello, L. P. & Norman, A. W. (2004). *Proc. Natl Acad. Sci. USA*, **101**, 1589–1594.